AGU PUBLICATIONS

JGR

Journal of Geophysical Research: Atmospheres

RESEARCH ARTICLE

10.1002/2013JD021339

Key Points:

- Significant warm-rain suppression with increasing aerosol
- Aerosol impact on rain rate agrees with aircraft measurements and models
- Aerosol impact on rain probability agrees well with multiscale climate model

Correspondence to:
J. A. L. Mann,
j.a.l.mann@pgr.reading.ac.uk

Citation:
Mann, J. A. L., J. C. Chiu, R. J. Hogan, E. J. O'Connor, T. S. L'Ecuyer, T. H. M. Stein, and A. Jefferson (2014), Aerosol impacts on drizzle properties in warm clouds from ARM Mobile Facility maritime and continental deployments, *J. Geophys. Res. Atmos.*, *119*, 4136–4148, doi:10.1002/2013JD021339.

Received 11 DEC 2013
Accepted 17 MAR 2014
Accepted article online 18 MAR 2014
Published online 9 APR 2014

Aerosol impacts on drizzle properties in warm clouds from ARM Mobile Facility maritime and continental deployments

Julian A. L. Mann[1], J. Christine Chiu[1], Robin J. Hogan[1], Ewan J. O'Connor[1,2], Tristan S. L'Ecuyer[3], Thorwald H. M. Stein[1], and Anne Jefferson[4]

[1]Department of Meteorology, University of Reading, Reading, UK, [2]Finnish Meteorological Institute, Helsinki, Finland, [3]Department of Atmospheric and Oceanic Sciences, University of Wisconsin-Madison, Madison, Wisconsin, USA, [4]Cooperative Institute for Research in Environmental Science, University of Colorado Boulder, Boulder, Colorado, USA

Abstract We have extensively evaluated the response of cloud base drizzle rate (R_{cb}; mm d^{-1}) in warm clouds to liquid water path (LWP; g m^{-2}) and to cloud condensation nuclei (CCN) number concentration (N_{CCN}; cm^{-3}), an aerosol proxy. This evaluation is based on a 19 month long data set of Doppler radar, lidar, microwave radiometers, and aerosol observing systems from the Atmospheric Radiation Measurement (ARM) Mobile Facility deployments at the Azores and in Germany. Assuming 0.55% supersaturation to calculate N_{CCN}, we found a power law $R_{cb} = (0.0015\pm0.0009)\cdot\mathrm{LWP}^{(1.68\pm0.05)} N_{CCN}^{-(0.66\pm0.08)}$, indicating that R_{cb} decreases by a factor of 2–3 as N_{CCN} increases from 200 to 1000 cm^{-3} for fixed LWP. Additionally, the precipitation susceptibility to N_{CCN} ranges between 0.5 and 0.9, in agreement with values from simulations and aircraft measurements. Surprisingly, the susceptibility of the probability of precipitation from our analysis is much higher than that from CloudSat estimates but agrees well with simulations from a multiscale high-resolution aerosol-climate model. Although scale issues are not completely resolved in the intercomparisons, our results are encouraging, suggesting that it is possible for multiscale models to accurately simulate the response of LWP to aerosol perturbations.

1. Introduction

Warm clouds in the boundary layer represent one of the main causes of the intermodel spread in climate projections, because models disagree substantially on how warm cloud coverage and properties will change in a warmer world and in turn feedback on surface temperature [*Bony et al.*, 2006; *Soden and Vecchi*, 2011]. Moreover, aerosols have a strong effect on climate via their potential to modify the properties of warm clouds; an increase in aerosol loading could reduce drizzle production, modulate the stability of the boundary layer, and change cloud properties, lifetime, and extent, which is referred to as the second aerosol indirect effect [*Albrecht*, 1989; *Pincus and Baker*, 1994; *Lohmann and Feichter*, 2005; *Feingold et al.*, 2010]. Recent studies showed that global models significantly overestimate drizzle frequency [*Stephens et al.*, 2010], which calls into question the fidelity with which the second aerosol indirect effect is captured [*Quaas et al.*, 2009].

Numerous modeling studies at a wide range of resolutions have shown drizzle suppression for warm clouds in polluted environments [e.g., *Ackerman et al.*, 2004; *Guo et al.*, 2011; *H. Wang et al.*, 2011; *M. Wang et al.*, 2011]. Intensive field campaigns for marine stratocumulus in the northeastern Atlantic [*Albrecht et al.*, 1995; *Wood*, 2005], the northeastern Pacific [*Stevens et al.*, 2003; *van Zanten et al.*, 2005; *Lu et al.*, 2007, 2009], and the southeastern Pacific [*Comstock et al.*, 2004; *Bretherton et al.*, 2010; *Wood et al.*, 2011] have also found evidence of an aerosol effect on drizzle suppression. These observational studies characterized the dependence of cloud base drizzle rate (R_{cb}) on liquid water path (LWP) and cloud droplet number concentration (N_d, being sensitive to aerosol perturbations), which were well reproduced with large-eddy simulations [*Geoffroy et al.*, 2008]. However, other metrics such as susceptibilities of precipitation intensity and probability to aerosol have not shown consistent agreement among observations and simulations [*Sorooshian et al.*, 2009, 2010; *Terai et al.*, 2012; *Feingold et al.*, 2013].

Precipitation susceptibility (S_R) is defined as follows:

$$S_R = -\frac{\partial \ln(R)}{\partial \ln(\alpha)}, \tag{1}$$

with fixed LWP, where R is precipitation rate and α is an aerosol proxy that is often N_d or aerosol index (AI; the product of aerosol optical depth and Ångström exponent). CloudSat observations of precipitating cumulus show that susceptibility S_R to AI monotonically increases with LWP up to 1000 g m^{-2}, similar to the susceptibility S_R to N_d in large-eddy simulations but with different magnitudes due to different choices of aerosol proxy [*Sorooshian et al.*, 2009]. In contrast, aircraft-based observations have shown a mostly flat response of S_R to N_d for precipitating clouds with LWP up to 300 g m^{-2}, and when incorporating nonprecipitating clouds, S_R decreases with LWP [*Terai et al.*, 2012]. *Feingold et al.* [2013] suggested that the time scale available for collision-coalescence processes in cloud systems could explain the different responses of S_R to aerosol proxy among simulations and observations. Other studies also point out that potential biases in estimates of S_R can arise from different choices of minimum R thresholds, spatial averaging scales, and cloud type among other factors [*Duong et al.*, 2011; *McComiskey and Feingold*, 2012; *Terai et al.*, 2012].

For susceptibility (S_{POP}) of the probability of precipitation (POP), defined as

$$S_{POP} = -\frac{\partial \ln(\mathrm{POP})}{\partial \ln(\alpha)}, \tag{2}$$

Wang et al. [2012] found that S_{POP} to AI in satellite observations was insensitive to LWP and 2–5 times smaller than that in climate models. Although these discrepancies could be partly attributed to the scale differences (as shown by *McComiskey and Feingold* [2012] for the aerosol impact on cloud albedo), this calls for more observational evidence to better understand how precipitation and POP susceptibilities change across a wide range of LWP.

In this paper, we analyze high temporal resolution observations of aerosols, clouds, and drizzle from the Atmospheric Radiation Measurement (ARM) Mobile Facility (AMF) deployments in the Black Forest, Germany, from April to December 2007 and at the Azores from June 2009 to December 2010. Through synergy between ground-based aerosol observing systems and active and passive remote-sensing instruments, we can examine aerosol-cloud-drizzle interactions with measurements that are collocated in a way that is difficult to replicate in satellite studies, and with higher spatiotemporal resolution than satellite and aircraft studies. In section 2, we outline the ground-based observations and methods used to perform our analysis. In section 3, first we provide observational constraints for the response of drizzle properties to aerosol perturbations in warm clouds, and then we examine whether the response from AMF data agrees with results from state-of-the-art satellite observations and climate models.

2. Ground-Based Observations at the Azores and the Black Forest

The AMF deployments at the Azores and in the Black Forest provide valuable information on marine and continental boundary layer clouds, respectively. During the Azores deployment, liquid precipitation, defined as a significant radar echo below ceilometer cloud base, occurred ~50% of cloudy times and was often in the form of virga, detailed by *Rémillard et al.* [2012]. Their study also found the most prevalent types of low clouds to be cumulus (20%), cumulus under stratocumulus (10–30%), and single-layer stratocumulus (10%). The dominant aerosol types were likely organic from long-distance continental pollution plumes and sea salt [*Pio et al.*, 2007; *Jefferson*, 2010], although sea salt generally contributes mainly to mass rather than to aerosol number concentration [*Blot et al.*, 2013]. Overall, aerosol amounts at the Azores were low; for a supersaturation of 0.55%, cloud condensation nuclei (CCN) number concentration (N_{CCN}) mainly ranged from 20 to 900 cm^{-3} with a peak at 250 cm^{-3}. In contrast, aerosol amounts during the Black Forest deployment were high and dominated by organic aerosols [*Jones et al.*, 2011]; N_{CCN} ranged mostly from 150 to 2300 cm^{-3} with a peak at 900 cm^{-3}. The occurrence of single-layer water clouds of interest was about 11% in the Black Forest [*Ebell et al.*, 2011].

This study focuses on interdependences between N_{CCN}, liquid water path (LWP), and drizzle rate at cloud base (R_{cb}). N_{CCN} was acquired from a Droplet Measurement Technologies CCN counter [*Roberts and Nenes*,

2005] positioned on a 10 m high mast, taking measurements every minute and cycling through seven supersaturations (S) from 0.1% to 1.2% on a 30 min basis. We discarded N_{CCN} measurements made immediately after the counter changed temperature or supersaturation because the counter is unstable at these times. As the Azores AMF was located near an airport, we also manually discarded data that were affected by exhaust during airplane maneuvers. For each 30 min cycle, the mean N_{CCN} for each S was computed and used in the relation $N_{CCN} = cS^k$ [*Twomey*, 1959] to derive fit parameters c and k, after which N_{CCN} can be calculated for a chosen S. In the following analysis, S was chosen to be 0.55% as a best estimate to reflect the low vertical velocities in marine boundary layer clouds [*Martin et al.*, 1994; *Hudson et al.*, 2010; *Wood*, 2012], and then linearly interpolated down from 30 min to 1 min resolution. At the Azores, mixing in the marine boundary layer is generally driven by cloud top longwave cooling, which does not depend strongly on the diurnal cycle, and so we assume that surface CCN measurements are representative of cloud base values over the entire diurnal cycle. At the Black Forest, where strong surface cooling at nighttime can create stable surface layers that prevent mixing of aerosol in the boundary layer, we limited our analysis to solar zenith angles less than 70°. This increases the likelihood that sufficient surface heating drives boundary layer mixing, and therefore that surface CCN measurements represent the cloud base values. Note that CCN data were unavailable at the Azores from January to mid-July 2010 due to an instrument fault.

LWP retrievals are available in the ARM Archive with an uncertainty of 20–30 g m^{-2} using the method of *Turner et al.* [2007]. The retrieval method optimizes LWP estimates by blending microwave radiometer measurements at 20 s resolution with radiosonde observations and radiative transfer calculations. This physically based method significantly reduces clear-sky bias, a common problem in earlier LWP retrievals. For our analysis, we excluded periods when the window of the microwave radiometer was wet as the resulting LWP retrievals were unreliable, and the period from mid-July to mid-August 2010 was also excluded due to an instrument fault. Finally, LWP was averaged to 1 min resolution, and any mean values below 20 g m^{-2} were discarded.

Drizzle rate below cloud, provided by Cloudnet [*Illingworth et al.*, 2007] with 30 s temporal and 43 m vertical resolution, is based on a synergy between 94 GHz Doppler radar and 524 nm backscatter lidar. The retrieval method exploits the fact that the ratio of radar to lidar backscatter power is proportional to the fourth power of mean drop size to characterize the drizzle drop size distribution, along with shape information from Doppler spectral width [*O'Connor et al.*, 2005]. The drizzle rate can then be estimated, given the drop size distribution and calculated drop terminal velocities, with an overall uncertainty of about 20%. Cloud base height from lidar, provided by Cloudnet, was used to select the cloud base drizzle rate R_{cb}, which was then averaged to 1 min resolution. Note that the radar was down for 23 days in September 2010 during the Azores deployment.

To ensure the representativeness of derived interdependences between LWP and drizzle rate, the LWP must correspond only to the lowest cloud layer and its associated drizzle detected by radar and lidar. Since the microwave radiometer is sensitive to the liquid water in all clouds in the profile, for cases with multiple liquid water cloud layers, the LWP is likely to be biased high for a given drizzle rate at lowest cloud base. Therefore, we restrict our analysis to single-layer warm clouds with bases above 170 m and tops lower than 3 km—similar to the criteria applied in *Rémillard et al.* [2012]—and geometrical thicknesses less than 1.5 km. The threshold of 1.5 km was chosen to minimize cases of multilayer precipitating clouds that are hard to separate by radar reflectivity alone and could be erroneously identified as a single-layer cloud. However, we include single-layer warm clouds with overlying cirrus at a height above the −40°C isotherm, as these cirrus clouds will not contain liquid water and so will not bias LWP in our analysis.

Figure 1 shows an example of measurements from AMF Azores for a single-layer stratocumulus cloud. The radar and lidar returns show clouds capped at around 2 km, and cloud geometric thickness deepened gradually from 0.3 km to 1 km during the period. During this deepening, LWP increased from below 100 g m^{-2} to above 300 g m^{-2} with a drizzle rate at cloud base of 0.5–1 mm d^{-1}; R_{cb} correlated well with LWP. For aerosol, N_{CCN} fluctuated between 200 and 350 cm^{-3}, representing a typical clean environment during the Azores campaign.

To minimize the influence of meteorological variability on the response of precipitation to aerosol perturbations, we stratified data by LWP. Ideally, if measurements in each bin are collected at time intervals sufficiently long to be independent, the sample mean is an unbiased estimate of the true mean with an

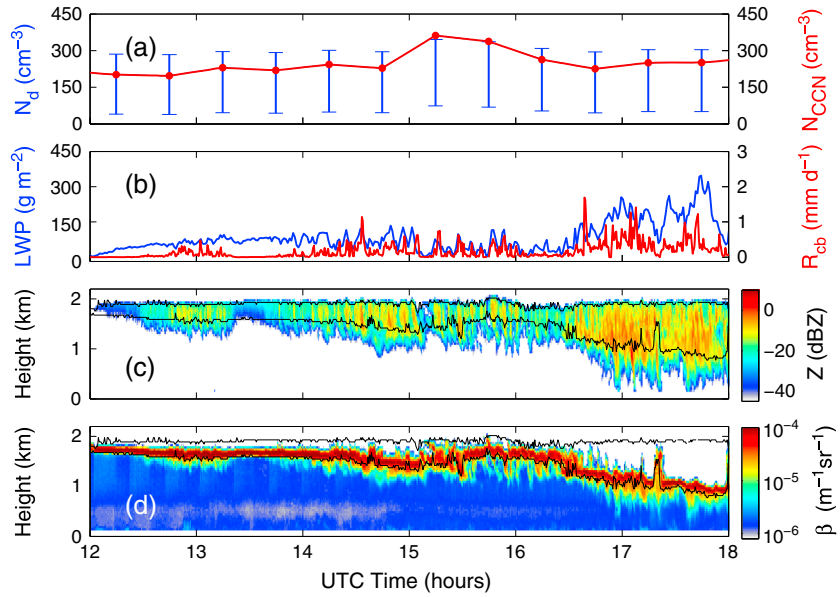

Figure 1. A subset of ARM Mobile Facility measurements on 29 November 2009 at AMF Azores. Time series of (a) cloud condensation nuclei (CCN) number concentration (N_{CCN}; red) and the potential range of cloud droplet number concentration derived from N_{CCN} (N_d; blue); and (b) cloud base drizzle rate (R_{cb}; red) and liquid water path (LWP; blue). The lower and higher bounds of N_d in Figure 1a are estimated using $N_d = 0.2 \cdot N_{CCN}$ from *Hudson and Yum* [2002] and $N_d = 0.38 \cdot N_{CCN} + 210$ from *Hegg et al.* [2012], respectively (see section 3.1 for details). Time-height plots of (c) radar reflectivity (Z) and (d) attenuated lidar backscatter (β); the black lines in the panels show cloud top from the radar and cloud base from the lidar.

uncertainty of the standard error. When measurements are collected at time intervals too short to be independent, the uncertainty increases as the total independent sample size reduces. To take account for the autocorrelation between samples in meteorological data sets, *Leith* [1973] characterized the time interval between independent samples as twice the *e*-folding time of the lagged time autocorrelation function. We analyzed the lagged time autocorrelation function for 1 min R_{cb} and found the time interval for independence to be 5 min. We then used this 5 min independent time interval to count the number of independent samples for each bin and calculated the standard error using the corresponding independent sample size.

3. Results

3.1. The Response of Drizzle Rate to LWP and N_{CCN}

After selecting single-layer warm clouds in the process described earlier, a 28 day long data set was obtained out of 19 months of available observations from the combined AMF deployments at Azores and the Black Forest. The Azores has relatively few occurrences of high N_{CCN} due to its marine location; the opposite is true of the continental Black Forest where low N_{CCN} is rare. To ensure that the response of R_{cb} to N_{CCN} is derived from a greater range of N_{CCN} than is possible at a single site, we combined data from both sites to maximize the number of N_{CCN} bins and the sample sizes in each N_{CCN} bin. As a result, the percentages of the total sample size in the lowest, middle, and highest N_{CCN} bin are approximately 40, 40, and 20.

Figure 2 shows mean R_{cb} as a function of LWP and N_{CCN} at 0.55% supersaturation. R_{cb} increases with LWP and decreases with N_{CCN}; the drizzle suppression by increasing aerosol is consistent with the hypothesis that greater N_{CCN} redistributes cloud water to more numerous and smaller droplets, reducing collision-coalescence rates. The suppression is also consistent with observations from satellite [*Lebsock et al.*, 2008; *L'Ecuyer et al.*, 2009], aircraft [e.g., *Lu et al.*, 2009], and ground-based instruments [*Comstock et al.*, 2004]. In general, R_{cb} decreases by a factor of 2–3 from the lowest to highest N_{CCN} bins across most LWP bins. Note that despite differences in typical N_{CCN} ranges between the Azores and Black Forest, the behavior of R_{cb} versus LWP at both sites individually is similar in the range between 300 and 600 cm^{-3} where both sites have ample samples.

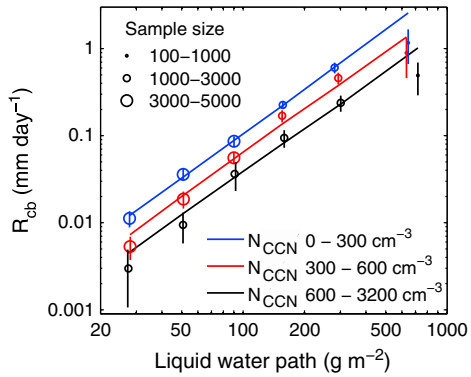

Figure 2. Cloud base drizzle rate R_{cb} as a function of liquid water path for various ranges of cloud condensation nuclei (CCN) number concentration (N_{CCN}). Mean N_{CCN} values for lowest to highest N_{CCN} bins are approximately 200, 430, and 1000 cm^{-3}. Symbols show bin-mean R_{cb} and LWP, with symbol size indicating the total sample size for each bin, and lines show a power law fit to the data (equation (3)). Error bars represent 95% confidence intervals accounting for sample autocorrelation. The percentage of the sample size in the lowest, middle, and highest N_{CCN} bins is approximately 40, 40, and 20, respectively. The six LWP bins are bounded by 20, 40, 70, 120, 210, 470, and 1700 g m^{-2}, respectively, containing 25, 25, 23, 15, 10, and 2% of the total samples.

Using the 18 bin-mean values of N_{CCN}, LWP, R_{cb}, and its standard error, from Figure 2, a weighted least squares fit to the natural logarithms of the data is performed. From this fit we obtain a power law,

$$R_{cb} = \gamma \mathrm{LWP}^{\alpha} N_{CCN}^{-\beta} = (0.0015 \pm 0.0009)\cdot \mathrm{LWP}^{(1.68\pm0.05)} N_{CCN}^{-(0.66\pm0.08)}, \quad (3)$$

which can be used to approximate the relationship between R_{cb} (mm d^{-1}), LWP (g m^{-2}), and N_{CCN} (cm^{-3}) at 0.55% supersaturation; the uncertainties in exponents α and β and the scaling factor γ represent 95% confidence intervals. These coefficients vary slightly with the choice of N_{CCN} bin widths but can be sensitive to supersaturation value S. For a range of S between 0.2 and 1%, the exponent of LWP (α) varies by less than 2%; the exponent of N_{CCN} (β) varies between 0.71 ± 0.08 and 0.48 ± 0.06, and γ varies between 0.0017 ± 0.0011 and 0.0007 ± 0.0004. While the exponent of LWP, α, of 1.68 agrees well with those observed from weakly precipitating stratocumulus clouds (e.g., 1.5–2 from *Pawlowska and Brenguier* [2003] and *van Zanten et al.* [2005]), comparison in exponent of N_{CCN} with literature is less straightforward because the widely used power laws were related to N_d rather than N_{CCN}. Since $N_d \propto N_{CCN}^c$, where c typically ranges between 0.5 and 1 [*Twomey*, 1974; *Hudson and Yum*, 2002; *Feingold et al.*, 2003; *McComiskey et al.*, 2009; *Sorooshian et al.*, 2009; *Hegg et al.*, 2012], the range of the exponent β between 0.48 and 0.71 for various supersaturations derived from AMF data corresponds to a range of the exponent of N_d between 0.48 and 1.42. This range spans the theoretical value (2/3) derived by *Kostinski* [2008] and *Feingold et al.* [2013] that assumed a unimodal drop size distribution, and values observed in *Pawlowska and Brenguier* [2003] and *van Zanten et al.* [2005] for weakly precipitating stratocumulus clouds. The range of N_d exponent (0.48–1.42) from AMF data provides further observational constraints on precipitation rate in models [*Abel et al.*, 2010; *Boutle and Abel*, 2012].

Since no measurements of N_d were obtained during the AMF deployments, we assume linearity between N_d and N_{CCN} at 0.55% supersaturation to allow us to compare the power law revealed in AMF measurements in Figure 2 to those from historical observations. We then estimated lower and upper bounds of N_d from N_{CCN} (see caption of Figure 1). The lower bound of N_d is based on measurements of cumulus in the Indian Ocean Experiment, predicting averaged N_d from N_{CCN} at 1% supersaturation [cf. *Hudson and Yum*, 2002, Table 2]; the upper bound is based on measurements of stratocumulus off the coasts of Chile, California, and Namibia, predicting peak N_d from N_{CCN} at 0.3% supersaturation [cf. *Hegg et al.*, 2012, Figure 2]. Next, we plotted AMF data along with historical campaign observations in Figure 3, using the relationship $R_{cb} \propto (\mathrm{LWP}/N_d)^{1.75}$ that was used to compare different field campaigns in *Lu et al.* [2009].

Figure 3 shows that data points with the lower bound of N_d overlap only with a few Atlantic Stratocumulus Transition Experiment (ASTEX) measurements that were previously considered outliers [*Wood*, 2005]; points with the upper bound of N_d agree reasonably well with the majority of historical observations, except those from the second Marine Stratus/Stratocumulus Experiment (MASE-II) over the eastern Pacific. However, this agreement should not be interpreted to mean that they have similar power law relationships. The straight lines drawn from such plots are affected not only by the exponents but also by the values of LWP and N_d themselves. The use of $(\mathrm{LWP}/N_d)^{1.75}$ is an attempt to compress the dependence of R_{cb} on two variables to be a function of just one. However, if a data set finds a very different exponent, as we have in the case of number concentration [and also *Pawlowska and Brenguier*, 2003], then little can be learned from such plots. Therefore, we argue that a more appropriate approach to evaluating the power law relationships is to plot the data in

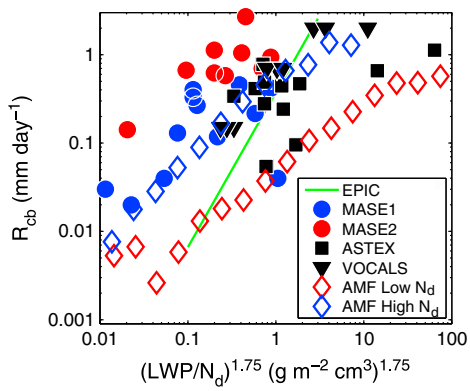

Figure 3. Relationship between observed cloud base drizzle rate R_{cb} and $(LWP/N_d)^{1.75}$, where LWP is liquid water path and N_d is cloud drop number concentration. AMF observations from this study represent a range bounded by the lowest and highest N_d estimated from *Hudson and Yum* [2002] and *Hegg et al.* [2012], respectively (see text for details). Past observations include measurements from Eastern Pacific Investigation of Climate [*Comstock et al.*, 2004], Marine Stratocumulus Experiment (MASE) I and II [*Lu et al.*, 2007, 2009], Atlantic Stratocumulus Transition Experiment (ASTEX) [*Wood*, 2005], and the Variability of the American Monsoon System (VAMOS) Ocean-Cloud-Atmosphere-Land Study Regional Experiment (VOCALS-REx) [*Bretherton et al.*, 2010].

the form used in Figure 2, which leads to the dependence of R_{cb} on both LWP and N_{CCN} (or N_d) being very clear.

To further investigate the sensitivity of R_{cb} to aerosol perturbations, we calculated precipitation susceptibility S_R to N_{CCN}, as in equation (1) where N_{CCN} is the aerosol proxy. Here the quantities R_{cb} and N_{CCN} are bin-mean values (as in Figure 2), and S_R is obtained by performing weighted least squares fits to the logarithms of R_{cb} and N_{CCN} at constant LWP, with 95% confidence intervals. Figure 4 shows that AMF-based S_R decreases from 0.9 to 0.5 with increasing LWP, consistent with the overall susceptibility of 0.66 for all LWP values found in equation (3). S_R values for the first three LWP bins are significant at the 0.05 level, while those for the last three bins are at the 0.15 level. The range of S_R also agrees to an extent with observations of stratocumulus from VOCALS-REx in the South East Pacific [*Terai et al.*, 2012], but we do not see an increase in S_R for LWP of around 80 g m^{-2}. Additionally, for LWP between 100 and 300 g m^{-2}, S_R agrees reasonably well with that from large-eddy simulations conducted for shallow precipitating cumulus clouds during the Rain In Cumulus over the Ocean (RICO) field experiment [*Sorooshian et al.*, 2009], although for RICO instances of small nonprecipitating clouds are removed, unlike in this study. This agreement supports the contention of *Sorooshian et al.* [2009] that clouds with LWP less than 500 g m^{-2} are less susceptible to aerosol because they lack sufficient total water to precipitate strongly; however, due to our limited sampling at high LWP, S_R from AMF data does not show the same increase at LWP higher than 500 g m^{-2} as shown in *Sorooshian et al.* [2009] and *Jiang et al.* [2010]. The different magnitudes and behaviors of S_R among studies may arise from the choice of aerosol proxies used in analyses. Therefore, attempts to use various aerosol proxies may help reconcile differences in S_R, although this is beyond the scope of this paper.

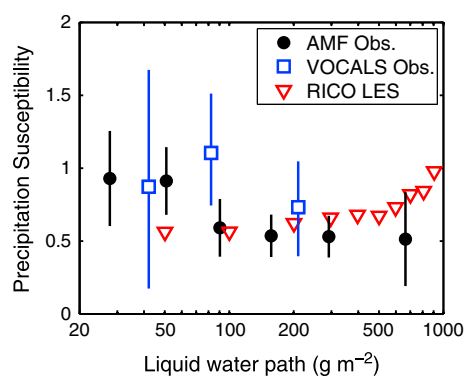

Figure 4. Precipitation susceptibility with respect to CCN number concentration as a function of liquid water path in AMF observations from this study and to cloud droplet number concentration in VOCALS observations averaged over a 5 km length scale (squares) [*Terai et al.*, 2012, Figure 7] and large-eddy simulations (LES, triangles; adapted from *Sorooshian et al.* [2009]) of precipitating cumulus initialized using soundings from the Rain in Cumulus over the Ocean (RICO) field campaign [*Rauber et al.*, 2007]. Error bars in AMF data represent 95% confidence intervals, which take into account the errors associated with R_{cb} in Figure 2.

3.2. Response of Precipitation Probability to Aerosol

The probability of precipitation (POP) is defined as the ratio of the number of rain events to the total number of cloudy events. Discrimination between rain and no-rain events can be performed based on radar reflectivity thresholds [*Liu et al.*, 2008], from −20 dB*Z* [*Mace and Sassen*, 2000] for continental drizzling clouds, −15 dB*Z* for light drizzling marine stratocumulus [*Terai et al.*, 2012], to 0 dB*Z* for "rain certain" events [*L'Ecuyer et al.*, 2009]. For the AMF data set, radar reflectivity of −15 dB*Z* and 0 dB*Z* corresponds to ~0.1 and ~1 mm d^{-1}, respectively. Using a radar reflectivity threshold of −15 dB*Z* and 0 dB*Z*, Figures 5a and 5b respectively show that POP decreases with chosen reflectivity threshold, and that POP increases with LWP and decreases with

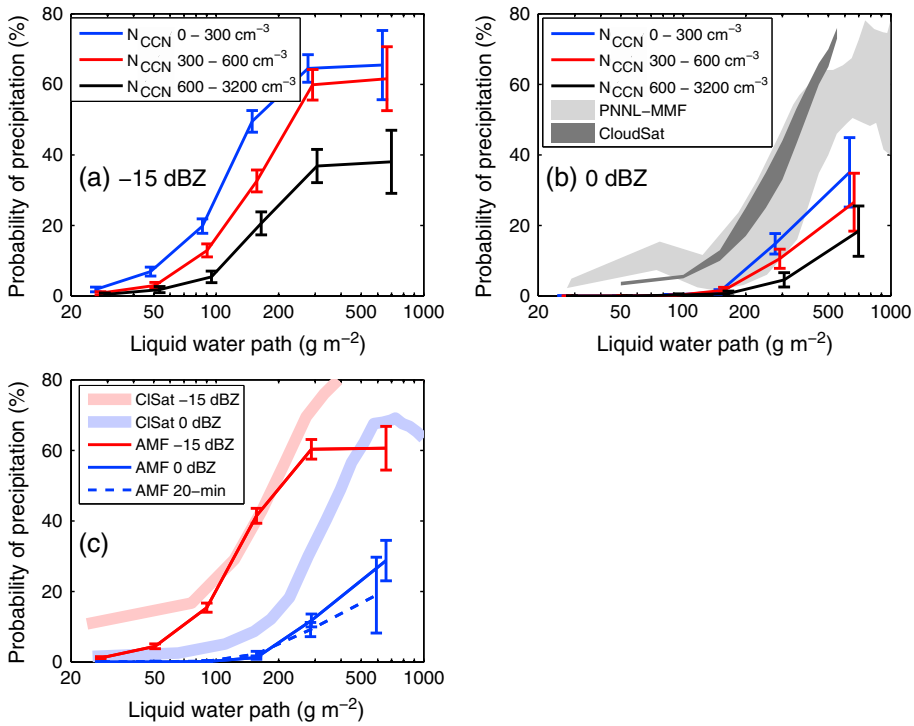

Figure 5. Probability of precipitation (%; POP) as a function of liquid water path (LWP) for various number concentrations of CCN, using a radar reflectivity threshold to determine a rain event of (a) −15 dB*Z*, and (b) 0 dB*Z*, including POP bounded by low and high aerosol index in stable atmospheric conditions from CloudSat observations [*L'Ecuyer et al.*, 2009] and from the PNNL-MMF multiscale climate model [*Wang et al.*, 2012]. (c) POP only for Azores region for −15 dB*Z* (red) and 0 dB*Z* (blue) reflectivity thresholds using CloudSat (thick lines) and AMF data (thin lines); the dashed thin blue line represents AMF LWP and POP averaged over longer time periods.

N_{CCN}, similar to the response of R_{cb} to N_{CCN} in Figure 2. For all LWP in Figure 5a and for LWP of 300 g m^{-2} in Figure 5b, there is a statistically significant difference in POP between low and high N_{CCN}, which has not been reported elsewhere and provides valuable observational evidence of an aerosol impact on POP.

Using the same reflectivity threshold of 0 dB*Z*, a similar response of POP to aerosol index (AI) was found using CloudSat and Advanced Microwave Scanning Radiometer—Earth Observing System (AMSR-E) measurements over oceans during 2007 [*L'Ecuyer et al.*, 2009]. Figure 5b shows that CloudSat-based POP increases with LWP and decreases with AI and agrees well with climate model simulations at 4 km scale from the multiscale aerosol-climate model PNNL-MMF (Pacific Northwest National Laboratory Multi-scale Model Framework) [*Wang et al.*, 2012]. However, a discrepancy exists in the magnitude of POP between AMF and CloudSat, which is not negligible and warrants further discussions.

First, to investigate a potential calibration issue between the CloudSat and AMF ground-based 94 GHz radars, we compared reflectivity versus height for warm clouds at least 100 m thick with tops below 3 km. From the CloudSat 2B-GEOPROF standard product [*Haynes and Stephens*, 2007], the cloud mask was first used to select warm clouds satisfying the above criteria from overpasses within a 4°×4° grid box around the AMF Azores site, and where the criteria were met, reflectivity profiles were selected. Then, AMF reflectivity profiles using the same criteria were sampled during a 4 h time window centered on the CloudSat overpass time; this way of comparing ground- and satellite-based radar reflectivity closely follows the intercomparison method of *Liu et al.* [2010]. Figure 6 shows the cumulative probability of reflectivity with height for both data sets. We find that the cumulative probabilities match well between the two, particularly for heights between 1200 m and 1800 m, suggesting there is no serious calibration issue.

For altitudes above 1800 m, CloudSat reflectivity tends to be higher than AMF at a given probability percentile. This is believed to be due to the long 480 m pulse of the CloudSat radar, which leads to range sidelobes extending above the clouds (see *Marchand et al.* [2008] and *Ceccaldi et al.* [2013] for further

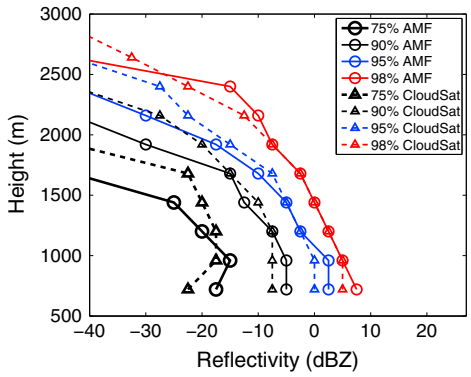

Figure 6. Curves of constant cumulative probability of reflectivity with height. At a given height the 95% curve, for example, intersects the value of reflectivity Z_i whereby 95% of samples at that height have a reflectivity less than or equal to Z_i. AMF Azores curves are shown by solid lines and circles, and CloudSat curves are shown by dashed lines and triangles.

discussions). An example of this is provided in Figure 7, which shows AMF radar measurements for 1 day when CloudSat overpassed near the Azores, with coplotted cloud tops from the CALIPSO vertical feature mask [*Vaughan et al.*, 2005]. The CloudSat cloud mask frequently identifies cloud up to 1 km above the cloud top heights from the CALIPSO mask and those detected by the AMF radar.

Unlike higher altitudes, any difference in the cumulative probability at lower altitudes between two data sets will have an impact on results in Figure 5b. Figure 6 shows that AMF reflectivity tends to be higher than CloudSat by 2.5 dB at altitudes below 1200 m at a given probability percentile, because the ability of CloudSat to detect cloud with confidence is reduced due to clutter [*Marchand et al.*, 2008]. Interestingly, this systematic reflectivity difference should make AMF data correspond to higher POP values (due to stronger radar reflectivity) than CloudSat, which is opposite to the finding in Figure 5b. Therefore, the calibration issue (if any) and the cloud mask problem cannot explain the discrepancy in POP between AMF and CloudSat data.

Second, to investigate whether the discrepancy in Figure 5b is due to regional variations in POP, we conducted the same analysis as *L'Ecuyer et al.* [2009] only for the region around the Azores (15–30°W; 30–45°N) in 2007–2010, shown in Figure 5c. Compared to Figure 5b, the relationships between POP and LWP from global oceans and the Azores are similar, consistent to the finding in *Tselioudis et al.* [2013] that the frequencies of occurrence of various cloud types in the Azores are surprisingly close to those observed globally. Additionally, the best agreement in POP between AMF and CloudSat occurs at lower LWP bins with a reflectivity threshold of −15 dB*Z*; however, the agreement degrades with increasing LWP and the reflectivity threshold used in rain event discrimination.

Relationships between POP and LWP from satellite observations vary with the choice of LWP retrievals used in the analysis. POP in Figures 5b and 5c is based on AMSR-E LWP retrieved from a footprint of 12 km. When using LWP from Moderate Resolution Imaging Spectroradiometer (MODIS) measurements with a fine spatial

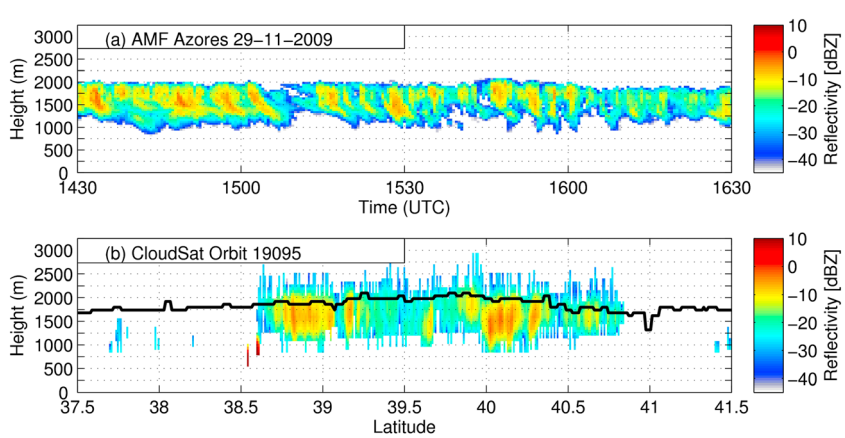

Figure 7. A comparison between AMF, CloudSat, and CALIPSO data around the Azores, showing (a) AMF radar reflectivity between 1430 and 1630 UTC on 29 November 2009, as also shown in Figure 1c, and (b) CloudSat reflectivity from Orbit 19095 on the same day, with overpass time at 1530 UTC over the Azores. The coplotted black line indicates the top of the liquid cloud layer identified in the CALIPSO vertical feature mask.

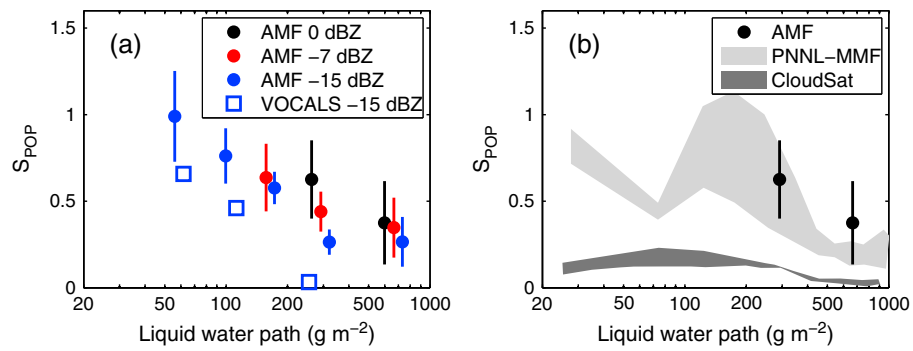

Figure 8. (a) Susceptibility of POP (S_{POP}) derived from AMF measurements using reflectivity thresholds of 0, −7 and −15 dB*Z*, compared with S_{POP} for the −15 dB*Z* threshold from the VOCALS-REx field campaign [*Terai et al.*, 2012, Figure 3]. (b) S_{POP} based on the 0 dB*Z* threshold from AMF compared to S_{POP} for different atmospheric stability regimes from CloudSat observations and the PNNL-MMF outputs at 4 km [*Wang et al.*, 2012].

resolution of 1 km, *Suzuki et al.* [2011] showed that 0 dB*Z* reflectivity threshold (cf. Figure 2) yielded 1% and 10% POP at LWP of 150 and 300 g m^{-2}, respectively, which agreed well with AMF data; however, the agreement degraded if a threshold of −15 dB*Z* was used. Since AMSR-E and MODIS-based LWPs are different not only in spatial scale but also in their retrieval principles that may lead to some systematic differences [*Seethala and Horváth*, 2010], it is unclear how much the spatial scale difference between AMSR-E and MODIS LWPs can be attributed to the discrepancy in POP. In short, POP from AMF data agrees better with results in *L'Ecuyer et al.* [2009] using −15 dB*Z* for drizzle discrimination, but agrees better with *Suzuki et al.* [2011] using 0 dB*Z*. Agreements are best for LWP lower than 300 g m^{-2}; for larger LWP, AMF-based POP values are substantially smaller than those from satellite observations, which can be partly due to the limitation of ground-based microwave radiometers in observing clouds with precipitation reaching the ground.

Third, to further investigate if the use of 1 min average AMF data has led to the discrepancy in POP, we averaged our LWP over 20 min periods to increase the AMF spatial scale from 600 m (with a nominal wind speed of 10 m s^{-1}) to 12 km, matching to the spatial scale of AMSR-E footprints. We also averaged radar reflectivity over 2 min periods to better match the 1.5 km footprint of CloudSat. The dashed blue line in Figure 5c shows that averaging over longer time periods not only slightly reduces POP but also shifts precipitating events into lower LWP bins, because reflectivity and LWP are smoothed to lower values. Clearly, a better match in the spatial scales among data products cannot help reduce the discrepancy in POP, which is broadly consistent with the spatial scale invariance shown in *Terai et al.* [2012] for clouds with geometric thickness greater than 200 m. However, we are aware that the attempt to represent statistics within CloudSat and AMSR-E footprints by averaging AMF data in 2–20 min time periods does not completely resolve the issue of spatial scale. A data set with a much longer time period can help obtain a greater sample size of 2–20 min averaged AMF data, which will in turn provide statistics that better represent those from 2-D footprints. For further investigation, such a data set could be provided by the recent addition of the Azores as a fixed observation site by the ARM Climate Research Facility.

After examining issues with calibration, spatial scale, and the use of radar reflectivity and LWP retrievals, results suggest that dedicated intercomparisons not only between ground-based and satellite observations but also among satellite observations themselves over focused regions and longer time periods will greatly help pin down the causes of the POP discrepancy. Furthermore, the ability for ground-based microwave radiometers to measure LWP in rainy conditions is needed to produce a more representative POP for clouds with large LWP.

3.3. Susceptibility of Precipitation Probability to Aerosol

Next, we examine the susceptibility of POP (S_{POP}), given in equation (2), where N_{CCN} is the aerosol proxy, suggested as a good indicator for evaluating the response of LWP to CCN perturbations in global climate models [*Wang et al.*, 2012]. To calculate S_{POP}, the same method as for calculating S_R is used but for the logarithm of POP and N_{CCN} at constant LWP. We excluded the sample size of rain events less than 20 in a bin, as it typically fails to show a convincing linear relationship of POP and N_{CCN} and can lead to unphysical S_{POP} estimates. Using various radar reflectivity thresholds for rain event discrimination, Figure 8a shows that S_{POP}

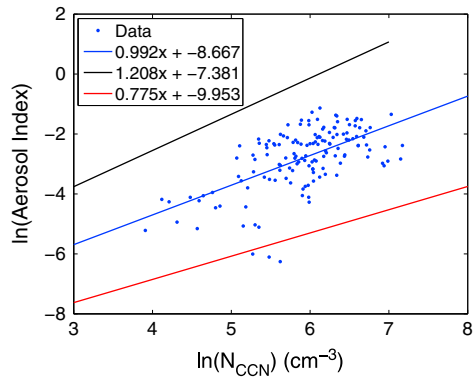

Figure 9. Relationships between CCN number concentration (N_{CCN}) and aerosol index (AI) from AERONET measurements during the AMF deployments at Azores, where N_{CCN} was taken at times within 1 h of an AI measurement. Blue points represent individual pairs of measurements; best fit linear regression to the data is shown by the blue line, with 95% confidence intervals shown by the black and red lines and $x = \ln(N_{CCN})$.

from AMF data mainly ranges between 0.2 and 1.0, and its response of S_{POP} to LWP can be sensitive to the reflectivity threshold used. With a lower threshold (i.e., −15 dB*Z*) and thus a larger raining sample size, Figure 8a shows that S_{POP} has smaller uncertainty and tends to decrease with LWP, similar to the finding in *Terai et al.* [2012] from aircraft observations in the southeast Pacific during VOCALS-REx. Since the autoconversion process dominates precipitation at low LWP while accretion rapidly becomes dominant at higher LWP, the decrease of S_{POP} with LWP suggests that aerosols more strongly influence precipitation initiation, in accord with other studies [e.g., *Wood et al.*, 2009; *Sorooshian et al.*, 2013].

Focusing again on the 0 dB*Z* threshold, Figure 8b shows that the magnitude of S_{POP} agrees well with PNNL-MMF, while the response of S_{POP} from CloudSat observations ranges between 0 and 0.2 and is relatively flat across all LWP bins [*Wang et al.*, 2012]. Such resemblance in S_{POP} response to LWP between AMF observations and MMF simulations is encouraging, but the difference in the use of aerosol proxy (AI versus N_{CCN}) can potentially alter the magnitude. To investigate the potential change in S_{POP} due to the different aerosol proxies, we approximated $\mathrm{AI} \propto N_{CCN}^{1.00 \pm 0.22}$ (Figure 9), using a matchup data set between N_{CCN} from AMF and AI estimates from Aerosol Robotic Network (AERONET) standard products [*Holben et al.*, 2001]. It follows that for a given AMF-observed S_{POP} of 0.5 in Figure 8b, the use of AI as the aerosol proxy changes S_{POP} to lie between 0.40 and 0.65, which still agrees with MMF simulations, although noise from scatter in the matchup between N_{CCN} and AI reduces the strength of the relationship and could potentially change S_{POP}. Since S_{POP} can be used to evaluate the modeled response of LWP to aerosol perturbations, the agreement in Figure 8b suggests that MMF simulations at a 4 km spatial scale appropriately capture the essence of aerosol-cloud-precipitation interactions shown in 1 min average AMF data.

4. Conclusions

We used a data set of 28 days duration selected from 19 months of observations from the ARM Mobile Facility deployments at the Azores and Black Forest, Germany to examine the response of cloud base drizzle rate (R_{cb}) to aerosol perturbations and liquid water path (LWP) for single-layer warm clouds below 3 km. High temporal resolution measurements from a collocated aerosol observing system, microwave radiometer, Doppler cloud radar, and lidar from the deployments were used to estimate CCN number concentration (N_{CCN}), LWP, and R_{cb}. This data set included precipitating and nonprecipitating cumulus and stratocumulus with LWP mainly less than 800 g m^{-2} and mean R_{cb} ranging from 0.005 mm d^{-1} to 1 mm d^{-1}. It also covered a wide range of N_{CCN}, mainly from 20 to 2300 cm^{-3}; the cleaner cases were mainly from the Azores maritime environment, while the more polluted cases were from the Black Forest continental site.

This study has led to several key findings. First, R_{cb} statistically significantly increases with LWP and decreases with N_{CCN}, supporting the concept of drizzle suppression by increasing aerosol and agreeing with many other observational and modeling studies. R_{cb}, associated with N_{CCN} greater than 600 cm^{-3}, was 2–3 times weaker than that with N_{CCN} less than 300 cm^{-3} across all LWP bins, indicating that drizzle suppression is robust. R_{cb} is proportional to $\mathrm{LWP}^{1.68\pm0.05}$ and $N_{CCN}^{-0.66\pm0.08}$ with an assumed supersaturation of 0.55%, as shown in equation (3), which can help to evaluate and constrain precipitation rate in models.

Second, the precipitation susceptibility S_R to N_{CCN} ranged between 0.5 and 0.9 and generally decreased with LWP. Although S_R values agree well with large-eddy simulations of shallow cumulus for LWP between 100 and 300 g m^{-2}, there is still a large degree of uncertainty in our precipitation susceptibility, which can be reduced by including more observations. This could potentially help increase the number of representative

N_{CCN} bins and thus help to reduce errors in S_R to tighten constraints on models. Additionally, analysis and intercomparisons of precipitation susceptibility to other aerosol proxies, such as cloud droplet number concentration, aerosol optical depth, and AI could help resolve outstanding discrepancies among various studies.

Third, similar to R_{cb}, the probability of precipitation (POP) also statistically significantly increases with LWP and decreases with N_{CCN}. POP using the -15 dBZ reflectivity threshold from AMF deployments agrees better with CloudSat-based POP that uses AMSR-E LWP, while better agreement in POP is seen with the CloudSat study using MODIS LWP when using the 0 dBZ threshold. AMF POP is also lower than POP from a high-resolution aerosol-climate model, although interestingly, the susceptibility of POP to N_{CCN} (S_{POP}) agrees well with each other and shows a sign of decrease with LWP. Since autoconversion (accretion) processes tend to dominate at low (high) LWP, this behavior in S_{POP} suggests that autoconversion-dominated precipitation is more susceptible to aerosol perturbations than accretion-dominated precipitation, as many suggested.

Finally, this study highlights the difference in S_{POP} between observations from ground-based, aircraft and satellites, and model simulations. S_{POP} from AMF data is higher than that from satellites and similar to S_{POP} from aircraft observations and a high-resolution climate model, which treats aerosol effects explicitly in an embedded cloud-resolving model. In particular, the similarity in S_{POP} with this model suggests that multiscale climate models may already be capable of representing aerosol-cloud-precipitation interactions well, and may not overestimate response of LWP to aerosol perturbations as originally thought. More studies, such as intercomparisons between high-resolution simulations, satellite observations, and ground-based observations at fixed sites for longer time periods and for various aerosol proxies, will help reduce uncertainties and provide confirmation of this.

Acknowledgments
This research was supported by a studentship from the UK Natural Environment Research Council (NERC; reference NE/I528569/1), and by grant DE-SC0007233 from the Office of Science (BER), U.S. Department of Energy. We would like to thank Robert Wood and the two anonymous reviewers for their thorough and helpful comments to improve our manuscript. We are very grateful to Thomas Bell and Jochen Broecker for their help with the statistics of our data set. We also thank Graham Feingold, Allison McComiskey, Chris Terai, Minghuai Wang, and Chris Westbrook for stimulating discussions and Colin O'Dowd and Ciaran Monahan for their helpful insight regarding ground-based instrumentation and aerosol measurements.

References

Abel, S. J., D. N. Walters, and G. Allen (2010), Evaluation of stratocumulus cloud prediction in the Met Office forecast model during VOCALS-Rex, *Atmos. Chem. Phys.*, *10*, 10,541–10,559.

Ackerman, A. S., M. P. Kirkpatrick, D. E. Stevens, and O. B. Toon (2004), The impact of humidity above stratiform clouds on indirect aerosol climate forcing, *Nature*, *432*(7020), 1014–1017, doi:10.1038/nature03174.

Albrecht, B. A. (1989), Aerosols, cloud microphysics, and fractional cloudiness, *Science*, *245*, 1227–1230, doi:10.1126/science.245.4923.1227.

Albrecht, B. A., C. S. Bretherton, D. W. Johnson, W. H. Schubert, and A. S. Frisch (1995), The Atlantic stratocumulus transition experiment ASTEX, *Bull. Am. Meteorol. Soc.*, *76*, 889–904.

Blot, R., A. D. Clarke, S. Freitag, V. Kapustin, S. G. Howell, J. B. Jensen, L. M. Shank, C. S. McNaughton, and V. Brekhovskikh (2013), Ultrafine sea spray aerosol over the southeastern Pacific: Open-ocean contributions to marine boundary layer CCN, *Atmos. Chem. Phys.*, *13*, 7263–7278.

Bony, S., et al. (2006), How well do we understand and evaluate climate change feedback processes?, *J. Clim.*, *19*, 3445–3482.

Boutle, I. A., and S. J. Abel (2012), Microphysical controls on the stratocumulus topped boundary-layer structure during VOCALS-REx, *Atmos. Chem. Phys.*, *12*, 2849–2863.

Bretherton, C. S., R. Wood, R. C. George, D. Leon, G. Allen, and X. Zheng (2010), Southeast pacific stratocumulus clouds, precipitation and boundary layer structure sampled along 20°S during VOCALS-REX, *Atmos. Chem. Phys.*, *10*, 10,639–10,654, doi:10.5194/acp-10-10639-2010.

Ceccaldi, M., J. Delanoë, R. J. Hogan, N. L. Pounder, A. Protat, and J. Pelon (2013), From CloudSat-CALIPSO to EarthCare: Evolution of the DARDAR cloud classification and its comparison to airborne radar-lidar observations, *J. Geophys. Res. Atmos.*, *118*, 7962–7981, doi:10.1002/jgrd.50579.

Comstock, K. K., R. Wood, S. A. Yuter, and C. S. Bretherton (2004), Reflectivity and rain rate in and below drizzling stratocumulus, *Q. J. R. Meteorol. Soc.*, *130*, 2891–2918, doi:10.1256/qj.03.187.

Duong, H. T., A. Sorooshian, and G. Feingold (2011), Investigating potential biases in observed and modeled metrics of aerosol-cloud-precipitation interactions, *Atmos. Chem. Phys.*, *11*, 4027–4037.

Ebell, K., S. Crewell, U. Lohnert, D. D. Turner, and E. J. O'Connor (2011), Cloud statistics and cloud radiative effect for a low-mountain site, *Q. J. R. Meteorol. Soc.*, *137*, 306–324.

Feingold, G., W. L. Eberhard, D. E. Veron, and M. Previdi (2003), First measurements of the Twomey indirect effect using ground-based remote sensors, *Geophys. Res. Lett.*, *30*(6), 1287, doi:10.1029/2002GL016633.

Feingold, G., I. Koren, H. Wang, H. Xue, and W. A. Brewer (2010), Precipitation-generated oscillations in open cellular cloud fields, *Nature*, *466*, 849–852, doi:10.1038/nature09314.

Feingold, G., A. McComiskey, D. Rosenfeld, and A. Sorooshian (2013), On the relationship between cloud contact time and precipitation susceptibility to aerosol, *J. Geophys. Res. Atmos.*, *118*, 10,544–10,554, doi:10.1002/jgrd.50819.

Geoffroy, O., J.-L. Brenguier, and I. Sandu (2008), Relationship between drizzle rate, liquid water path and droplet concentration at the scale of a stratocumulus cloud system, *Atmos. Chem. Phys.*, *8*, 4641–4654.

Guo, H., J.-C. Golaz, and L. J. Donner (2011), Aerosol effects on stratocumulus water paths in a PDF-based parameterization, *Geophys. Res. Lett.*, *38*, L17808, doi:10.1029/2011GL048611.

Haynes, J. M., and G. L. Stephens (2007), Tropical oceanic cloudiness and the incidence of precipitation: Early results from CloudSat, *Geophys. Res. Lett.*, *34*, L09811, doi:10.1029/2007GL029335.

Hegg, D. A., D. S. Covert, H. H. Jonsson, and R. K. Woods (2012), A simple relationship between cloud drop number concentration and precursor aerosol concentration for the regions of Earth's large marine stratocumulus decks, *Atmos. Chem. Phys.*, *12*, 1229–1238.

Holben, B. N., et al. (2001), An emerging ground-based aerosol climatology: Aerosol optical depth from AERONET, *J. Geophys. Res.*, *106*(D11), 12,067–12,097, doi:10.1029/2001JD900014.

Hudson, J. G., and S. S. Yum (2002), Cloud condensation nuclei spectra and polluted and clean clouds over the Indian Ocean, *J. Geophys. Res.*, *107*(D19), 8022, doi:10.1029/2001JD000829.

Hudson, J. G., S. Noble, and V. Jha (2010), Stratus cloud supersaturations, *Geophys. Res. Lett.*, *37*, L21813, doi:10.1029/2010GL045197.

Illingworth, A. J., et al. (2007), Continuous evaluation of cloud profiles in seven operational models using ground-based observations, *Bull. Am. Meteorol. Soc.*, *88*, 1–16, doi:10.1175/BAMS-88-6.

Jefferson, A. (2010), Empirical estimates of CCN from optical properties at four remote sites, *Atmos. Chem. Phys.*, *10*, 6855–6861, doi:10.5194/acp-10-6855-2010.

Jiang, H., G. Feingold, and A. Sorooshian (2010), Effect of aerosol on the susceptibility and efficiency of precipitation in warm trade cumulus clouds, *J. Atmos. Sci.*, *67*, 3525–3540.

Jones, H. M., J. Crosier, A. Russell, M. J. Flynn, M. Irwin, T. W. Choularton, H. Coe, and G. McFiggans (2011), In situ aerosol measurements taken during the 2007 COPS field campaign at the hornisgrinde ground site, *Q. J. R. Meteorol. Soc.*, *137*, 252–266, doi:10.1002/qj.727.

Kostinski, A. B. (2008), Drizzle rates versus cloud depths for marine stratocumuli, *Environ. Res. Lett.*, *3*, doi:10.1088/1748-9326/3/4/045019.

Lebsock, M. D., G. L. Stephens, and C. Kummerow (2008), Multisensor satellite observations of aerosol effects on warm clouds, *J. Geophys. Res.*, *113*, *D15205*, doi:10.1029/2008JD009876.

L'Ecuyer, T. S., W. Berg, J. Haynes, M. Lebsock, and T. Takemura (2009), Global observations of aerosol impacts on precipitation occurrence in warm maritime clouds, *J. Geophys. Res.*, *114*, D09211, doi:10.1029/2008JD011273.

Leith, C. E. (1973), The standard error of time-average estimates of climatic means, *J. Appl. Meteorol.*, *12*, 1066–1069, doi:10.1175/2009JAS3071.1.

Liu, Y., B. Geerts, M. Miller, P. Daum, and R. McGraw (2008), Threshold radar reflectivity for drizzling clouds, *Geophys. Res. Lett.*, *35*, L03807, doi:10.1029/2007GL031201.

Liu, Z., R. Marchand, and T. Ackerman (2010), A comparison of observations in the tropical western Pacific from ground-based and satellite millimeter-wavelength cloud radars, *J. Geophys. Res.*, *115*, D24206, doi:10.1029/2009JD013575.

Lohmann, U., and J. Feichter (2005), Global indirect aerosol effects: A review, *Atmos. Chem. Phys.*, *5*, 715–737.

Lu, M.-L., W. C. Conant, H. H. Jonsson, V. Varutbangkul, R. C. Flagan, and J. H. Seinfeld (2007), The marine stratus/stratocumulus experiment (MASE): Aerosol-cloud relationships in marine stratocumulus, *J. Geophys. Res.*, *112*, D10209, doi:10.1029/2006JD007985.

Lu, M.-L., A. Sorooshian, H. H. Jonsson, G. Feingold, R. C. Flagan, and J. H. Seinfeld (2009), Marine stratocumulus aerosol cloud relationships in the MASE-II experiment: Precipitation susceptibility in eastern Pacific marine stratocumulus, *J. Geophys. Res.*, *114*, D24203, doi:10.1029/2009JD012774.

Mace, G. G., and K. Sassen (2000), A constrained algorithm for retrieval of stratocumulus cloud properties using solar radiation, microwave radio-meter, and millimeter cloud radar data, *J. Geophys. Res.*, *105*, 29,099–29,108.

Marchand, R., G. G. Mace, T. Ackerman, and G. L. Stephens (2008), Hydrometeor detection using CloudSat—An Earth-orbiting 94-GHz cloud radar, *J. Atmos. Oceanic Technol.*, *25*, 519–533.

Martin, G., D. Johnson, and A. Spice (1994), The measurement and parameterization of effective radius of droplets in warm stratocumulus clouds, *J. Atmos. Sci.*, *51*, 1823–1842.

McComiskey, A., and G. Feingold (2012), The scale problem in quantifying aerosol indirect effects, *Atmos. Chem. Phys.*, *12*(2), 1031–1049, doi:10.5194/acp-12-1031-2012.

McComiskey, A., G. Feingold, A. S. Frisch, D. D. Turner, M. A. Miller, J. C. Chiu, Q. L. Min, and J. A. Ogren (2009), An assessment of aerosol-cloud interactions in marine stratus clouds based on surface remote sensing, *J. Geophys. Res.*, *114*, doi:10.1029/2008JD011006.

O'Connor, E. J., R. J. Hogan, and A. J. Illingworth (2005), Retrieving stratocumulus drizzle parameters using Doppler radar and lidar, *J. Appl. Meteorol.*, *44*, 14–27.

Pawlowska, H., and J.-L. Brenguier (2003), An observational study of drizzle formation in stratocumulus clouds for general circulation model (GCM) parameterizations, *J. Geophys. Res.*, *108*(D15), 8630, doi:10.1029/2002JD002679.

Pincus, R., and M. B. Baker (1994), Effect of precipitation on the albedo susceptibility of clouds in the marine boundary-layer, *Nature*, *372*, 250–252, doi:10.1038/372250a0.

Pio, C. A., et al. (2007), Climatology of aerosol composition (organic versus inorganic) at nonurban sites on a west-east transect across Europe, *J. Geophys. Res.*, *112*, D23S02, doi:10.1029/2006JD008038.

Quaas, J., et al. (2009), Aerosol indirect effects—General circulation model intercomparison and evaluation with satellite data, *Atmos. Chem. Phys.*, *9*, 8697–8717.

Rauber, R. M., et al. (2007), Rain in shallow cumulus over the ocean: The RICO campaign, *Bull. Am. Meteorol. Soc.*, *88*, 1912–1928.

Rémillard, J., P. Kollias, E. Luke, and R. Wood (2012), Marine boundary layer cloud observations at the Azores, *J. Clim.*, *25*, 7381–7398.

Roberts, G. C., and A. Nenes (2005), A continuous-flow streamwise thermal-gradient CCN chamber for atmospheric measurements, *Aer. Sci. Tech.*, *39*, 206–221, doi:10.1080/027868290913988.

Seethala, C., and Á. Horváth (2010), Global assessment of AMSR-E and MODIS cloud liquid water path retrievals in warm oceanic clouds, *J. Geophys. Res.*, *115*, D13202, doi:10.1029/2009JD012662.

Soden, B., and G. Vecchi (2011), The vertical distribution of cloud feedback in coupled ocean-atmosphere models, *Geophys. Res. Lett.*, *38*, L12704, doi:10.1029/2011GL047632.

Sorooshian, A., G. Feingold, M. D. Lebsock, H. Jiang, and G. L. Stephens (2009), On the precipitation susceptibility of clouds to aerosol perturbations, *Geophys. Res. Lett.*, *36*, L13803, doi:10.1029/2009GL038993.

Sorooshian, A., G. Feingold, M. D. Lebsock, H. Jiang, and G. L. Stephens (2010), Deconstructing the precipitation susceptibility construct: Improving methodology for aerosol-cloud precipitation studies, *J. Geophys. Res.*, *115*, D17201, doi:10.1029/2009JD013426.

Sorooshian, A., Z. Wang, G. Feingold, and T. S. L'Ecuyer (2013), A satellite perspective on cloud water to rain water conversion rates and relationships with environmental conditions, *J. Geophys. Res. Atmos.*, *118*, 6643–6650, doi:10.1002/jgrd.50523.

Stephens, G., T. L'Ecuyer, R. Forbes, A. Gettlemen, J.-C. Golaz, A. Bodas-Salcedo, K. Suzuki, P. Gabriel, and J. Haynes (2010), Dreary state of precipitation in global models, *J. Geophys. Res.*, *115*, D24211, doi:10.1029/2010JD014532.

Stevens, B., et al. (2003), Dynamics and chemistry of marine stratocumulus - DYCOMS-II, *Bull. Am. Meteorol. Soc.*, *84*, doi:10.1175/BAMS-84-5.579.

Suzuki, K., G. L. Stephens, S. C. van den Heever, and T. Y. Nakajima (2011), Diagnosis of the warm rain process in cloud-resolving models using joint CloudSat and MODIS observations, *J. Atmos. Sci.*, *68*, 2655–2670, doi:10.1175/JAS-D-10-05026.1.

Terai, C. R., R. Wood, D. C. Leon, and P. Zuidema (2012), Does precipitation susceptibility vary with increasing cloud thickness in marine stratocumulus?, *Atmos. Chem. Phys.*, *12*, 4567–4583.

Tselioudis, G., et al. (2013), Global weather states and their properties from passive and active satellite cloud retrievals, *J. Clim.*, *26*, 7734–7746.

Turner, D. D., S. A. Clough, J. C. Liljegren, E. E. Clothiaux, K. E. Cady-Pereira, and K. L. Gaustad (2007), Retrieving liquid water path and precipitable water vapor from the atmospheric radiation measurement (arm) microwave radiometers, *IEEE Trans. Geosci. Remote Sens.*, *45*, 3680–3690, doi:10.1109/tgrs.2007.903703.

Twomey, S. (1959), The nuclei of natural cloud formation: Part II: The supersaturation in natural clouds and the variation of cloud droplet concentration, *Pure Appl. Geophys.*, *43*, 243–249.
Twomey, S. (1974), Pollution and planetary albedo, *Atmos. Environ.*, *8*, 1251–1256.
van Zanten, M. C., B. Stevens, G. Vali, and D. L. Lenschow (2005), Observations of drizzle in nocturnal marine stratocumulus, *J. Atmos. Sci.*, *62*, 88–106.
Vaughan, M., D. Winker, and K. Powell (2005), CALIOP Algorithm Theoretical Basis Document, Part 2: Feature detection and layer properties algorithms, PC-SCI-202.01, 87 pp., NASA Langley Res. Cent., Hampton, VA. [Available at http://www-calipso.larc.nasa.gov/resources/project_documentation.php.]
Wang, H., P. J. Rasch, and G. Feingold (2011), Manipulating marine stratocumulus cloud amount and albedo: A process-modelling study of aerosol-cloud-precipitation interactions in response to injection of cloud condensation nuclei, *Atmos. Chem. Phys.*, *11*, 4237–4249.
Wang, M., S. Ghan, M. Ovchinnikov, X. Liu, R. Easter, E. Kassianov, Y. Qian, and H. Morrison (2011), Aerosol indirect effects in a multi-scale aerosol-climate model PNNL-MMF, *Atmos. Chem. Phys.*, *11*, 5431–5455, doi:10.5194/acp-11-5431-2011.
Wang, M., et al. (2012), Constraining cloud lifetime effects of aerosols using A-Train satellite observations, *Geophys. Res. Lett.*, *39*, L15709, doi:10.1029/2012GL052204.
Wood, R. (2005), Drizzle in stratiform boundary layer clouds. Part I: Vertical and horizontal structure, *J. Atmos. Sci.*, *62*, 3011–3033.
Wood, R. (2012), Stratocumulus clouds, *Mon. Weather Rev.*, *140*, 2373–2423, doi:10.1175/MWR-D-11-00121.1.
Wood, R., T. L. Kubar, and D. L. Hartmann (2009), Understanding the importance of microphysics and macrophysics for warm rain in marine low clouds. Part II: Heuristic models of rain formation, *J. Atmos. Sci.*, *66*, 2973–2990, doi:10.1175/2009JAS3072.1.
Wood, R., et al. (2011), The VAMOS Ocean-Cloud-Atmosphere-Land Study Regional Experiment (VOCALS-REX): Goals, platforms, and field operations, *Atmos. Chem. Phys.*, *11*, 627–654, doi:10.5194/acp-11-627-2011.